

3-D finite element modelling of prestressed hollow-core slabs strengthened with near surface mounted CFRP strips

Karam Mahmoud^{1,2a}, Puneet Anand^{1b} and Ehab El-Salakawy^{*1}

¹Department of Civil Engineering, University of Manitoba, Winnipeg, Manitoba, Canada

²Department of Civil Engineering, Assuit University, Assuit, Egypt

(Received October 21, 2017, Revised February 6, 2018, Accepted February 7, 2018)

Abstract. A non-linear finite element model (FEM) was constructed using a three-dimensional software (ATENA-3D) to investigate the effect of strengthening on the behavior of prestressed hollow-core (PHC) slabs with or without openings. The slabs were strengthened using near surface mounted (NSM)-carbon fiber reinforced polymer (CFRP) strips. The constructed model was validated against experimental results that were previously reported by the authors. The validated FEM was then used to conduct an extensive parametric study to examine the influence of prestressing reinforcement ratio, compressive strength of concrete and strengthening reinforcement ratio on the behavior of such slabs. The FEM results showed good agreement with the experimental results where it captured the cracking, yielding, and ultimate loads as well as the mid-span deflection with a reasonable accuracy. Also, an overall enhancement in the structural performance of these slabs was achieved with an increase in prestressing reinforcement ratio, compressive strength of concrete, external reinforcement ratio. The presence of openings with different dimensions along the flexural or shear spans reduced significantly the capacity of the PHC slabs. However, strengthening these slabs with 2 and 4 (64 and 128 mm² that represent reinforcement ratios of 0.046 and 0.092%) CFRP strips was successful in restoring the original strength of the slab and enhancing post-cracking stiffness and load carrying capacity.

Keywords: hollow-core slabs; strengthening; openings; near surface mounted technique; CFRP strips finite element modeling

1. Introduction

Prestressed hollow-core (PHC) slabs are widely used in parking garages and industrial buildings due to their lightweight and favorable structural performance. These structures usually undergo changes during their service life such as increased load intensity or provision of openings to accommodate intake/exhaust ducts or utility conduits or require restoration if they are deteriorating. Therefore, strengthening of different components of the building is required to meet the new requirements. Carbon fiber reinforced polymer (CFRP) materials offer a viable option for the restoration or strengthening of existing structures especially those exposed to harsh environments that is due to their chemical and physical properties, including their light weight, resistance to corrosion, outstanding fatigue strength, high strength, reduced maintenance cost and ease of installation (FIB bulletin 2001, ISIS Canada 2007).

Strengthening of PHC slabs can be done either with externally bonded (EB) technique or near surface mounted (NSM) technique. The EB technique requires surface

treatment as a pre-requisite prior to its application. The NSM technique involves making grooves in the surface of concrete substrate then the CFRP strips are inserted inside the grooves using an appropriate adhesive (De Lorenzis *et al.* 2000). Premature debonding is regarded as one of the drawbacks of EB technique, which makes it less preferable, compared to the NSM technique. Protection against fire, external agents of corrosion and deterioration, and better bond between the FRP and concrete substrate are some of the advantages of using NSM technique for strengthening. The bond behavior of an NSM-FRP bar/strip is different from that of an EB-FRP laminate mainly because: (1) the NSM FRP strip has a much larger area of bonded interface as the FRP strip is surrounded by concrete on three sides; (2) significant confinement to the FRP strip is provided by the surrounding concrete. While these two features generally lead to larger bond strength of NSM-FRP bars/strips, they also make the bond behavior more complicated. Thus, the selection of an appropriate bond model for employing the NSM-FRP technique is essential. Several research studies have been conducted to investigate the bond between the NSM reinforcement and concrete substrate, and feasibility and advantages of NSM technique over EB one (Teng *et al.* 2006, Al-Saadi *et al.* 2015, Mousavi and Dehestani 2015, Al-Saadi and Al-Mahaidi 2016). Test of simply supported RC members strengthened with NSM strips have shown that NSM strengthening elements debond or fail at significantly higher strain than EB strengthening systems; therefore, in general, NSM strengthened members are expected to have a much more

*Corresponding author, Professor
E-mail: Ehab.El-Salakawy@umanitoba.ca

^aPost-Doctoral Fellow
E-mail: karam.mahmoud@eng.au.edu.eg

^bMSc Student
E-mail: anandp3@myumanitoba.ca

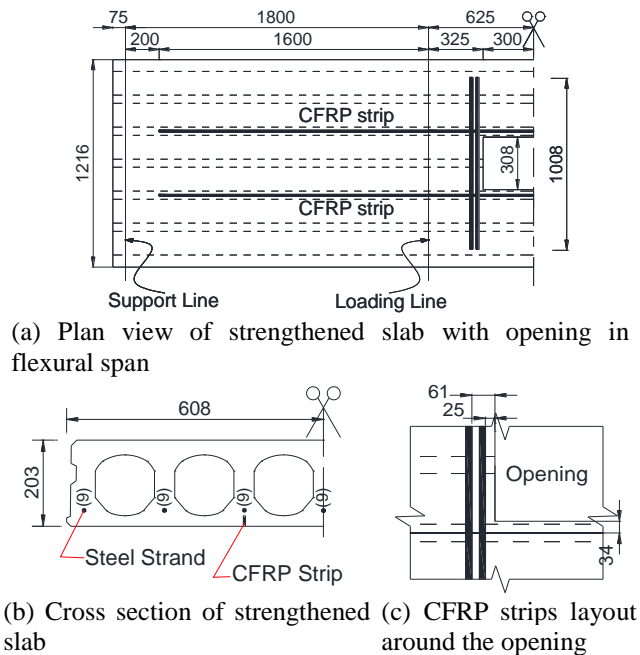


Fig. 1 Details of test slabs and strengthening layout (all dimensions are in mm)

ductile behavior than those strengthened with EB (Hassan and Rizkalla, 2003, Taljsten *et al.* 2003, Kim and Riyad 2004, Barros *et al.* 2007). A study was carried out on PHC slabs where six full-scale slabs were strengthened in positive bending moment region with CFRP strips and tested to failure under monotonic loading. The slab dimensions were 1,200 mm width, 120 mm depth and 3,550 mm total length over a clear span of 3,200 mm. The slabs were internally reinforced with six pre-tensioned strands of 6 mm diameter each. It was found that uniform crack patterns and a high strengthening efficiency were achieved when using NSM-CFRP strips (El-Gabbas *et al.* 2009).

Furthermore, the creation of openings in PHC slabs leads to considerable reduction in the load carrying capacity, energy dissipation capacity, stiffness and ductility of these slabs. The effect of openings on the ultimate load carrying capacity and failure mechanisms was studied using a 3D non-linear FEM (Khajehdehi and Panahshahi 2016). The model was first validated against the results of previously conducted experiments on RC slabs without openings. Afterwards, openings with variable sizes (6.26, 14 and 25% of the floor panel area) were considered. It was concluded that the failure mechanisms were different, where yielding of the bars around the opening corners is critical to the overall behavior of the slabs. Also, Enochsson *et al.* (2007) carried out a research study involving the use of CFRP strips for strengthening of two-way steel-RC slabs, two opening sizes measuring 0.85×0.85 and 1.2×1.2 m were considered in both experimental and analytical studies. The slabs were square with a side length of 2.6 m and an overall depth of 100 mm. All strengthened slabs achieved a higher ultimate load carrying capacity than the control specimen (without opening). In addition, the CFRP-strengthened slab in the experiment exhibited higher stiffness in comparison with the reference slabs.

This study is an extension of an experimental investigation on the strengthening of PHC slabs strengthened with NSM technique that was conducted by the authors' research team (Foubert *et al.* 2016, Mahmoud *et al.* 2017). The experimental study investigated the effect of strengthening of slabs with or without openings on their behavior and strength. In this numerical study, the effect of a wide range of parameters on the behavior of such slabs is presented. A summary of the experimental study and the main findings are provided below.

2. Summary of the experimental program

2.1 Test specimens

Eleven PHC full-scale slabs were constructed and tested under four-point bending up to failure. The test specimens had a thickness of 203 mm and a total length of 5,000 mm (Fig. 1). The design of test specimens complied with CSA/A23.3-14 (CSA 2014a) and CSA S6/14 (CSA 2014b) to meet the flexural and shear requirements. For the CFRP-strengthened slabs, the strengthened capacity was calculated using the strain-compatibility method as prescribed in the CSA/S806-12 (CSA 2012). Each specimen was designed to simulate a typical full-scale prestressed roof or floor member. All test specimens had a shear span to-depth ratio of 11.4. The test specimens were identified using the format I-1-S0-NO, where the roman numeral 'I' indicates the test series (I, II, III), the number '1' represents the level of prestressing (1 or 2 for prestressing reinforcement area of 383.5 and 515.3 mm², respectively), the 'S0' denotes the number of strips that were used as an external reinforcement (S2, S4, and S8 for slabs strengthened with 2, 4 and 8 CFRP strips, respectively), and the last part of the name indicates the presence and type of in-situ opening (NO: No Opening, FO : Flexural span opening, and SO : Shear span opening). The details of the experimental test slabs are shown in Table 1.

2.2 Material properties

All specimens were cast using normal weight, ready-mixed concrete with a target compressive strength of 28 MPa at 18 hours and 45 MPa at 28 days. The reinforcement used to prestress all slabs was 7-wire low-relaxation high-strength steel strands of grade 1,860. The applied prestressing force was varied by changing the reinforcement ratio using different diameter of strands. The used CFRP strips (rectangular section of 2×16 mm) had a tensile strength, modulus of elasticity, and rupture strain of 2,068 MPa, 131 GPa, and 0.017, respectively.

2.3 Test setup and instrumentation

The slabs were tested in a standard four-point bending setup, selected to maximize the constant moment region along the mid-span. Steel bearing plates having a width of 50 mm were used as end supports. The bearing plates were supported by roller support in one side and hinged support on the other. The clear span of the test specimens (4,850

Table 1 Details of test specimens

Specimen	Concrete Compressive strength (MPa)	Prestressing Reinforcement area (mm ²)	External Reinforcement area (mm ²)	Opening Location
I-1-S0-NO	64		N/A	N/A
I-1-S2-NO	56	384	64	N/A
I-1-S4-NO	64		128	N/A
I-1-S8-NO	64		256	N/A
I-2-S0-NO	56		N/A	N/A
I-2-S2-NO	56	515	64	N/A
I-2-S4-NO	56		128	N/A
II-1-S0-FO	64		N/A	Flexural span
II-1-S0-SO	56	384	N/A	Shear span
III-1-S2-FO	56		64	Flexural span
III-1-S2-SO	56		64	Shear span

mm) was divided into a pure bending middle span (1,250 mm) and two shear spans (1,800 mm each). The instrumentation comprised of linear variable differential transducers (LVDTs), PI-gauges and strain gauges. The LVDTs were used to monitor the deflection along the longitudinal profile of the test specimens. The strain gauges were installed along the prestressing steel reinforcement and external reinforcement (NSM-CFRP strips) to capture the induced strains. More details about the layout of the instrumentation can be found in Foubert *et al.* (2016), Mahmoud *et al.* (2017).

2.4 Main findings

Test results indicated that the NSM-CFRP strengthening technique effectively enhanced both the flexural and shear capacities of PHC slabs. The improvement in ultimate capacity was reduced in slabs that failed due to shear before attaining their full flexural capacity. Also, strengthening openings with NSM-CFRP strips not only restored the flexural strength deficit incurred because of cutting the openings and the prestressing strand but also provided additional flexural capacity. Moreover, the strengthened slabs showed an increase in both deflection ductility and energy ductility of PHC slabs. However, the increase in both types of ductility in slabs failed in shear were less than those in slabs failed in flexure-shear. More detailed test results and discussions can be found elsewhere (Foubert *et al.* 2016, Mahmoud *et al.* 2017).

3. Finite Element Modelling (FEM)

3.1 Reinforcement

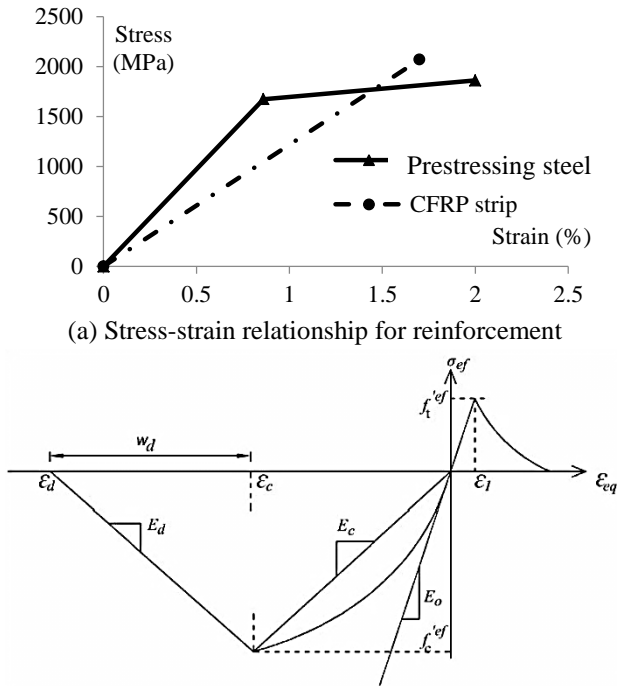
For the modeling of reinforcing bars, a truss element was used. The truss element is suitable for plane 2D as well as 3-D analysis problems. The selection of truss elements was a must so that prestressing forces could be applied. Two distinctive material types were used for the modelling of prestressing and NSM reinforcement (Fig. 2(a)). A bi-linear stress-strain with strain hardening relationship was considered for the prestressing reinforcement.

The software allows applying the prestressing force to reinforcement; therefore, the force was applied to prestressing strands considering the losses calculated for each slab. For the NSM-CFRP strips, a linear elastic stress-strain curve was defined. The CFRP strips were modeled in the form of discrete reinforcement bars possessing the equivalent area of FRP strips/sheets. The CFRP strips used in this study had dimensions of 2 mm in thickness, and 16 mm width (nominal area of 32 mm²). The CFRP strips around openings were modeled similar to the laboratory experiments (Mahmoud *et al.* 2017). In the experiments, all longitudinal CFRP strips were placed such that the strip width (16 mm) was in the vertical direction, while in the transverse direction, the strips were running underneath the longitudinal ones with their width in the horizontal direction. The properties of reinforcement provided in Table 2 were used in the FEM.

3.2 Concrete material

For modelling of concrete, a built-in fracture-plastic constitutive model was used. The fracture model is developed using the Rankine failure criterion while the plastic model is primarily based on the Menetrey-William failure surface. Thus, this distinctive fracture-plastic model is capable of combining both plastic and fracture models in a single model which can employ plasticity to simulate crushing of concrete and fracture mechanics to simulate cracking of concrete. This model also takes into account the effect of plastic deformation, material nonlinearity and cracking in 3-D. Some of the significant features of this model are the reduction in compressive strength after cracking, non-linearity in compression considering softening and hardening, effect of tension stiffening, and bi-axial strength failure criterion.

A nonlinear elastic approach based on the equivalent uniaxial law (Fig. 2(b)) is used for deriving the material stiffness matrix. In this approach, the stress-strain relationship of the concrete before the peak stress can be used for both normal and high strength concrete. After attaining peak compressive stress, the softening part (descending branch of the stress-strain curve) is linear. A perfectly elastic behavior of concrete in the un-cracked zone is considered; however, after cracking, the stress-strain



(a) Stress-strain relationship for reinforcement
 (b) Stress-strain law for Concrete (Cervenka et al. 2013)
 Fig. 2 Constitutive models for reinforcement and concrete

relationship in tension follows the exponential crack opening law. The mathematical values for the constitutive model are dependent on the concrete compressive strength. Therefore, the concrete compressive strength is the only property of concrete that is required by the program. More details about this model can be found elsewhere (Cervenka et al. 2016).

3.3 Bearing plates

Similar to laboratory experiments, steel plates were used for supports and loading spreader beams during the numerical modelling. Distribution and transfer of stresses were the primary objectives of those steel plates. An elastic isotropic element was used for simulating these steel plates. The material used for the plates was linear-elastic possessing 200 GPa modulus of elasticity and Poisson's ratio of 0.3.

3.4 Bond models for reinforcement-concrete interface

The selection of proper bond models for modelling the bond between concrete and reinforcement is essential. The commercial software package enables the use of predefined bond models for steel (prestressing) reinforcement. The selected bond model (Fig. 3(a)) in this study was based on the work of (Bigaj 1999). This model accounts for reinforcement type, reinforcement diameter, compressive strength of concrete and bond quality to predict the bond-slip relationship.

A bond model proposed by Zhang et al. (2013) was used for the NSM-CFRP strips in this study. In this model, the concrete compressive strength and the groove height-to-width ratio are the two key parameters. The bond-slip

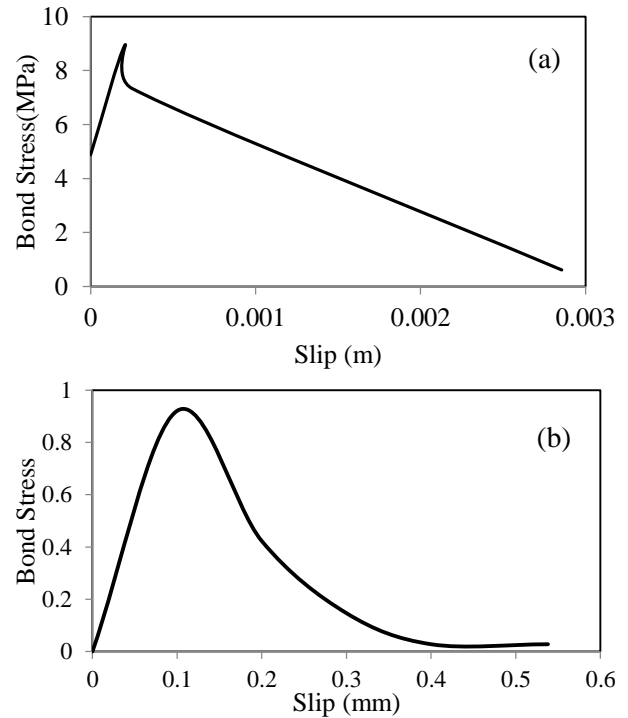


Fig. 3 Bond model for (a) steel strands (Bigaj 1999) and (b) CFRP strips (Zhang et al. 2013)

model (Fig. 3(b)) is able to predict accurate interfacial fracture energy and the appropriate shape of bond-slip curve, which are the two major aspects associated with an efficient bond model. The simplified equation for bond-slip relationship is of the following form:

The system examined, shown schematically in Fig. 1 is a beam of variable cross section, carrying a so called heavy tip mass M . Its mass moment of inertia with respect to the perpendicular axis at the centroid S is denoted by J_S . The publications (Abolghasemi and Jalali 2003, Younesian and Esmailzadeh 2010, Arvin and Bakhtiari-Nejad 2011) are considered also with rotating beams in which nonlinear oscillations are investigated. Analytical and experimental

$$\tau = A \left(\frac{2B - s}{B} \right)^2 \sin \left(\frac{\pi}{2} \cdot \frac{2B - s}{B} \right) \quad (1)$$

where $s \leq 2B$

In the above equation, τ and s are the bond stress and corresponding slip, respectively, while A and B are two constants, which can be determined as follows

$$A = 0.72 \gamma^{0.138} f'_c{}^{0.613} \quad (2)$$

$$B = 0.37 \gamma^{0.284} f'_c{}^{0.006} \quad (3)$$

where γ = groove height-to-width, and f'_c = concrete compressive strength.

3.5 Model geometry and boundary conditions

The numerical model was constructed to simulate the full size of test specimens so that openings at different locations can be created. Irregular voids present in the hollow-core slabs were modelled using a set of lines and 3-

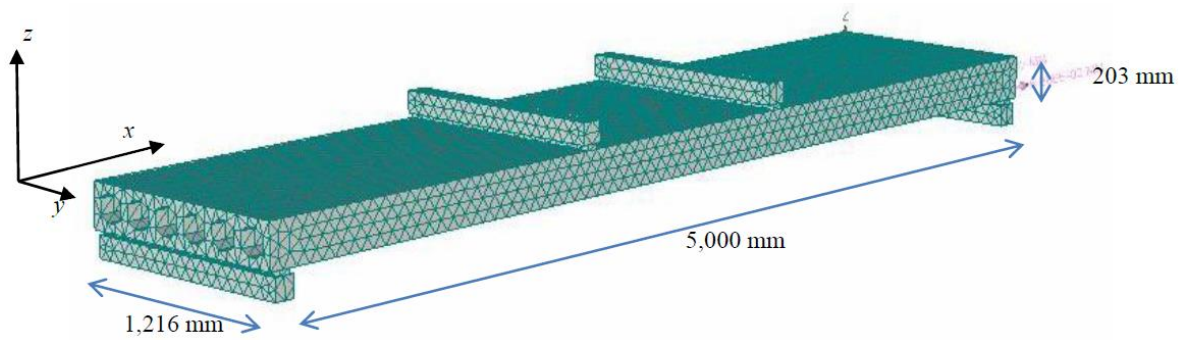


Fig. 4 Finite element modeling and meshing of test slab

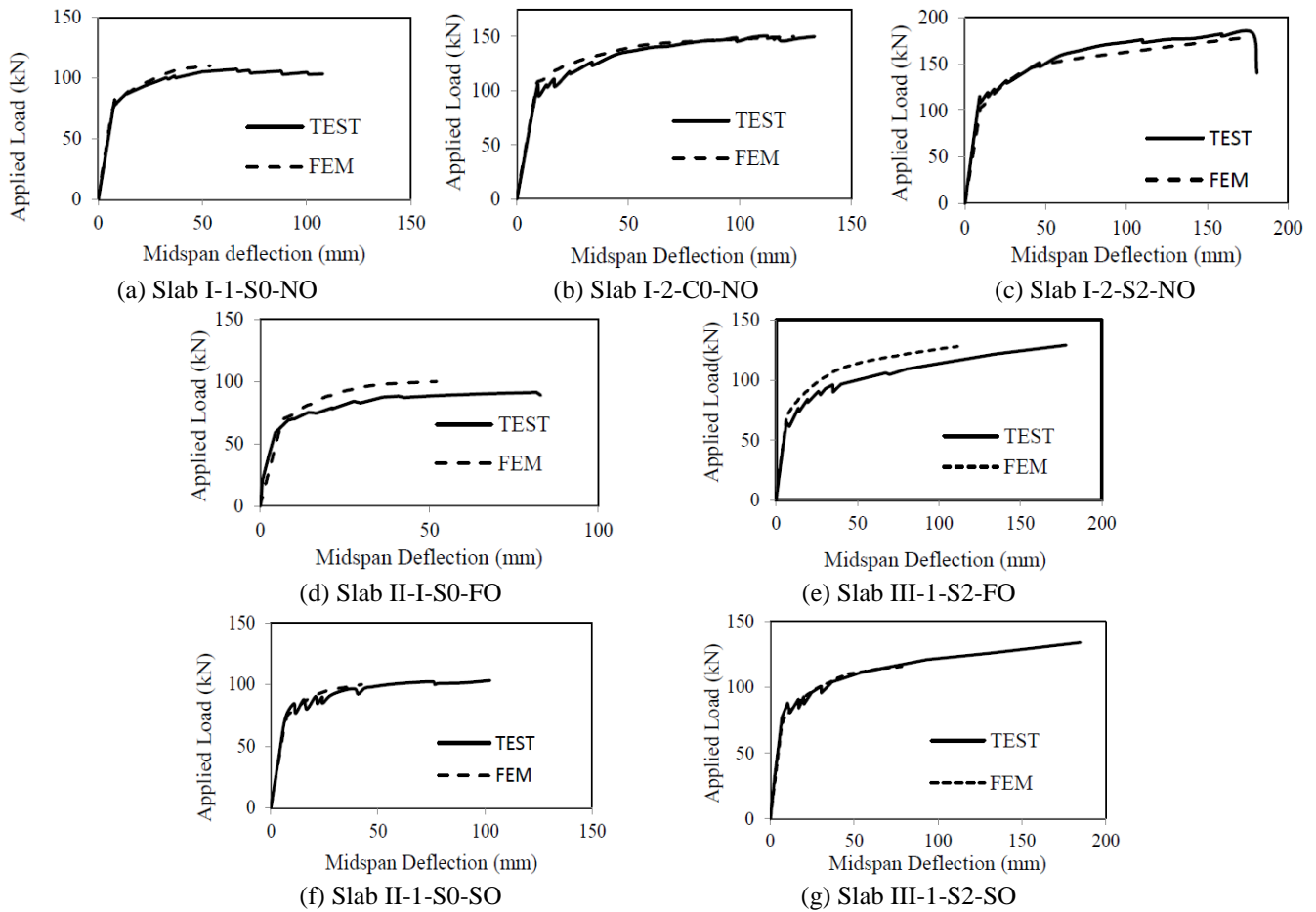


Fig. 5 Validation of FE model against the experimental test results

point arc. The ATENA-3D software has two built-in elements for modelling concrete; (i) brick and (ii) tetrahedral elements. Brick elements are more suitable for analysis of prismatic RC members. Since the PHC slabs comprised of irregular voids and complex geometries (as openings were also present), it was not possible to use brick elements with this regard. As such, the tetrahedral element was used in the finite element modelling. It is a simple and efficient element to discretize structures with non-planar surfaces or complex geometries. A preliminary study was conducted to evaluate the effect of mesh size on the finite element results.

The main objective was to find the suitable mesh size to achieve a reasonable balance between accuracy of results

and number of elements in the model which dramatically affects the required computing space and processing time to converge. Several trials were conducted using different mesh sizes ranging from 25 to 100 mm. However, mesh sizes larger than 50.75 mm were found to yield inaccurate results with a higher level of variance. On the other hand, mesh size less than 50.75 mm did not result in higher accuracy but increased the convergence time significantly, making it less optimal. Therefore, a mesh size of 50.75 mm was selected. The support conditions during the analytical modelling were selected in such a manner that one end of the specimen behaved as a hinged support while the other end acted like a roller support. The translations in x , y , and z directions were restricted in case of the hinged

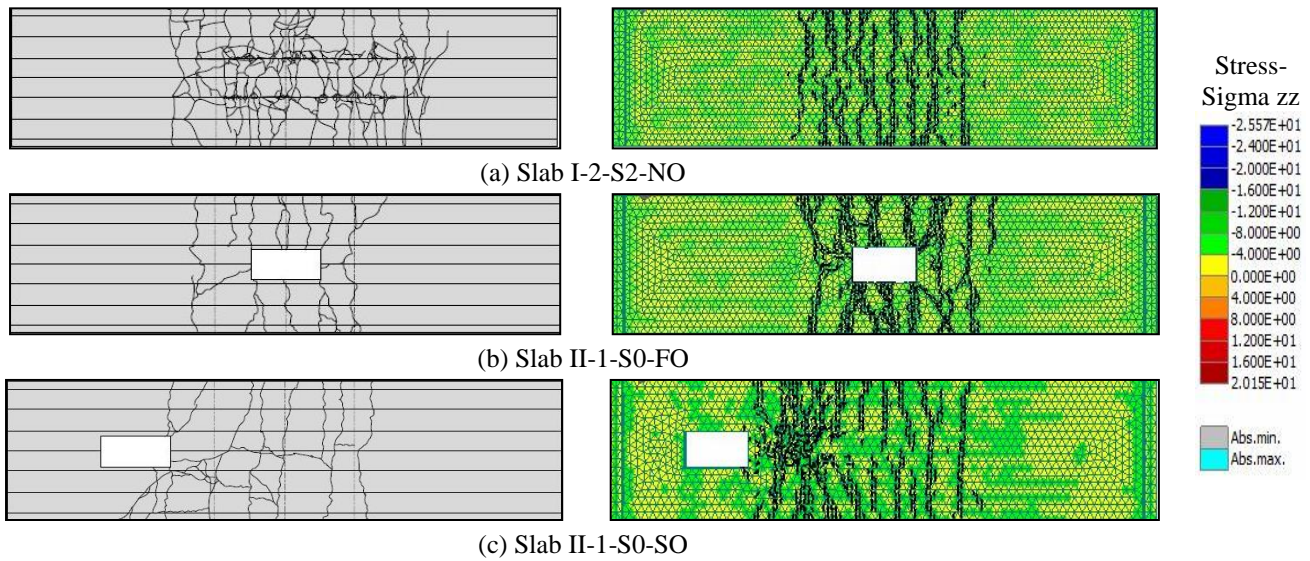


Fig. 6 Experimental versus FEM cracking pattern for selected specimens at failure

support. For the roller support, the translation in x direction was allowed while the translations in y and z directions were prevented. In both, hinge and roller, the rotation about y axis was allowed. The modified Newton-Raphson method was used during the analysis where stiffness matrix was adjusted to consider the non-linear changes in geometry at the end of each step.

4. FEM validation

The obtained data from the constructed FEM were validated against the experimental results of the previously tested PHC slabs. Seven specimens were chosen for the validation process. The PHC slabs selected for the validation process were representative of the different parameters investigated in the experimental study. Fig. 5 shows that the global behavior, in terms of the load-deflection relationship, of the seven slabs obtained from the numerical analysis was similar to the experimental results. The FEM predicted reasonably the pre-cracking flexural stiffness as well as the post-cracking flexural stiffness with respect to the experimental specimens and reached ultimate capacities within reasonable accuracy (less than 10%). Fig. 6 also depicts the cracking patterns of slabs I-2-S2-NO and II-1-S0-FO at failure, which are similar to those obtained from the FEM. The cracking load and pre-cracking stiffness was accurately predicted for all laboratory specimens using the numerical model. The FEM cracking load was approximately 4.3% less than the corresponding experimental one. Also, the yielding of prestressing reinforcement took place at a load comparable to the experimental one (in the range of 92 to 105%). Regarding the ultimate capacities, slabs tested analytically failed at 110, 150, 177, 98, 127, 100 and 119 kN which represent 97, 100, 103, 92, 98, 99, and 90% of the experimental ultimate load, for specimens I-1-S0-NO, I-2-S0-NO, I-2-S2-NO, II-1-S0-FO, III-1-S2-FO, II-1-S0-SO and III-1-S2-SO, respectively.

Fig. 6 depicts the cracking pattern as observed for (a) slab I-2-S2-NO, (b) slab II-1-S0-FO and (c) slab II-1-S0-SO. These slabs represented the cases for strengthening and provision of openings on flexural and shear span. It was thus evident from the comparison with experimental results of these slabs that the constructed FEM could predict the cracking pattern accurately. In general, the FEM was reasonably able to predict the behavior of such slabs; thus, it was then used to run the parametric study.

5. Parametric study

The FEM used in this parametric study has the same geometric details, material properties and other relevant properties as those selected for the validation process. The variable considered for the parametric study included the effect of compressive strength of concrete, prestressing reinforcement ratio, CFRP-NSM reinforcement ratio and the dimensions of openings on the strength and structural behavior of the PHC slabs. The nomenclature of all specimens contains four parts. The first part refers to the concrete compressive strength (56, 64, 80, and 100 MPa) while the second part denotes the prestressing reinforcement ratio (2, 2.7, 3.7 and 6.4 for a reinforcement ratio of 0.002, 0.0027, 0.0037, 0.0064, respectively). The third part stands for the number of the CFRP strips used to strengthen the slab. The fourth part refers to the location ("F" for flexural span and "S" for shear span) and dimensions of openings (1, 2, 3 and 4 for opening with $308 \times 600 \text{ mm}^2$, $308 \times 308 \text{ mm}^2$, $450 \times 308 \text{ mm}^2$, and $600 \times 308 \text{ mm}^2$, respectively). For example, Specimen 64-2-C2-F1 indicates a slab with a concrete compressive strength of 64 MPa, a prestressing reinforcement ratio of 0.002, strengthened with two CFRP strips and had an opening size of $308 \times 600 \text{ mm}^2$ along the flexural span.

In the discussion presented below, the mode of failure of the specimens was identified as follows. In case of unstrengthened slabs, the mode of failure was determined

Table 2 Specimen details and results for series I

Specimen	Prestressing reinforcement		Concrete strength, (MPa)	Cracking load, (kN)	Yielding load, (kN)	Ultimate Capacity, (kN)	Mode of Failure
	Area, (mm ²)	Ratio					
64-2.0-C0-NO			64	64	78	84	F
80-2.0-C0-NO	275	0.002	80	66	80	88	F
100-2.0-C0-NO			100	70	84	92	F
64-3.7-C0-NO			64	108	142	150	F-S
80-3.7-C0-NO	517	0.0037	80	116	154	160	F-S
100-3.7-C0-NO			100	128	156	166	F-S
64-6.4-C0-NO			64	146	233	238	F-S
80-6.4-C0-NO	898	0.0064	80	162	244	258	F-S
100-6.4-C0-NO			100	176	248	272	F-S

Note: F = Flexural failure; F-S = Flexure-shear failure

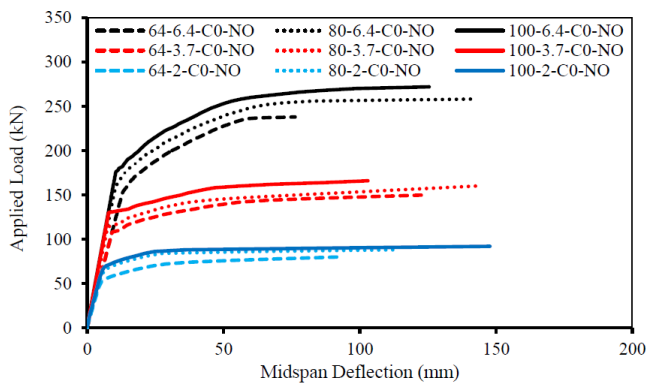


Fig. 7 Load-deflection relationship for series I

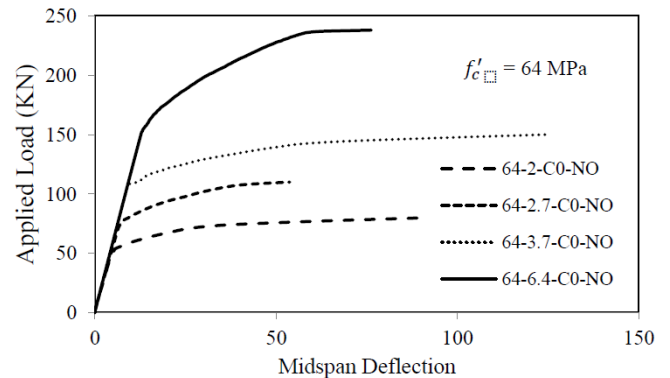


Fig. 8 Load-deflection relationship for series II

using the cracking pattern along with the obtained strains in prestressing strands. For the strengthened slabs, in addition to those mentioned above, the mode of failure in the CFRP was confirmed by using the strains in the CFRP strips as compared to those measured experimentally.

5.1 Effect of compressive strength of concrete

The considered concrete compressive strength ranged between 64 to 100 MPa. This range of concrete strength was studied for slabs with three different prestressing reinforcement ratios of 0.002, 0.0037 and 0.0064. Table 2 summarizes the details of all FEM specimens in this series (I) along with the obtained results.

As expected, it was observed that both the pre-cracking and the post-cracking stiffness increased with the increase in the compressive strength (Fig. 7). For the slab with prestressing reinforcement ratio of 0.002, increasing the compressive strength of concrete from 64 to 100 MPa increased the cracking load by 10%. For the same increase in the concrete strength, the cracking load increased by approximately 19 and 21% for the specimen with a prestressing reinforcement ratio of 0.0037 and 0.0064, respectively. Similarly, an increase in yielding and ultimate load was observed as the concrete strength increased (Table 2). For example, the yielding load was 146, 162 and 176 kN for specimens 64-6.4-0-NO, 80-6.4-0-NO, and 100-6.4-0-NO, respectively. All slabs studied analytically in this series showed a slight increase in the ultimate capacity when compressive strength of concrete was increased. The

ultimate load increased by 7 and 5% (on average for the three different reinforcement ratios) when the concrete strength increased from 64 to 80 MPa and from 80 to 100 MPa. Regarding the mode of failure, the increase in compressive strength of concrete did not affect the mode of failure. Thus, Specimens 64-2-C0-NO, 80-2-C0-NO and 100-2-C0-NO failed in pure flexure after yielding of prestressing reinforcement. Specimens with prestressing reinforcement ratios of 0.0037 and 0.0064 experienced a mixed mode of failure as yielding of reinforcement was followed by sudden shear failure.

5.2 Effect of prestressing reinforcement ratio

The selected specimens to study the effect of prestressing reinforcement ratio were representative of different prestressing reinforcement ratios as prescribed by the local supplier of the PHC slabs. Four different reinforcement ratios (0.002, 0.0027, 0.0037, and 0.0064) were selected in this study, including the prestressing reinforcement ratios that were used during verification of the numerical model (Table 3).

Fig. 8 shows the load-deflection relationship for the PHC slabs with different prestressing reinforcement ratios. During the initial stages of loading, the slabs remained uncracked and a perfectly elastic behavior was observed. However, after reaching the cracking load, the response of the slab tends to be non-linear until yielding is attained. Afterwards, excessive deflection took place with slight increase in the load until failure. Increasing the

Table 3 Specimen details and results for Series II

Specimen	Prestressing reinforcement		Concrete strength, (MPa)	Cracking load, (kN)	Yielding load, (kN)	Ultimate Capacity, (kN)	Mode of Failure
	Area, (mm ²)	Ratio					
64-2.0-C0-NO	275	0.0020	64.1	64	78	84	F
80-2.0-C0-NO	384	0.0027		78	104	110	F
100-2.0-C0-NO	517	0.0037		108	142	150	F-S
64-3.7-C0-NO	898	0.0064		146	233	238	F-S

Note: F = Flexural failure; F-S = Flexure-shear failure

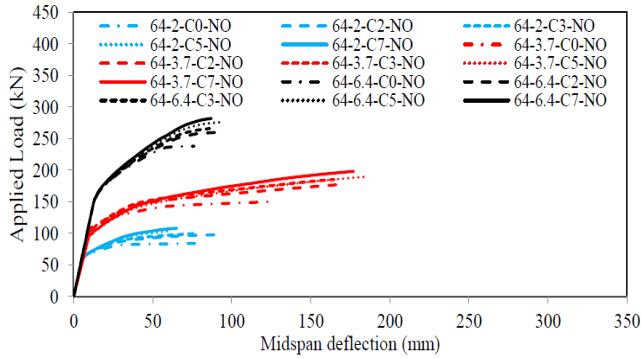


Fig. 9 Load-deflection relationship for series III

reinforcement ratio enhanced the post-cracking stiffness significantly, which resulted in lower deflection at the same load level. After cracking, the tensile reinforcement begins to play a major role in the flexural stiffness of the slab. The post-cracking stiffness increased significantly with increasing the prestressing reinforcement ratio.

It was also noted that increasing the prestressing reinforcement ratio from 0.002 to 0.0027 resulted in an increase in the cracking load from 60 to 78 kN (30% increase). When the prestressing reinforcement ratio increased from 0.0027 to 0.0037, the increase in the cracking load was 38% (from 78 to 108 kN). The increase in the cracking load for the slab containing the highest reinforcement ratio of 0.0064 was approximately 35% greater than the specimen having the moderate reinforcement ratio of 0.0037. A sharp increase in cracking load was thus evident with the increase in prestressing reinforcement ratio. Yielding load also exhibited a similar increase when the prestressing reinforcement ratio was increased. An increase in the prestressing reinforcement ratio from 0.002 to 0.0027 and further from 0.0027 to 0.0037 increased the yielding load by 33 and 37%, respectively. The highest yielding load was attained for Specimen 64-6.4-C0-NO at 238 kN, thereby indicating an increase of 65% with respect to Specimen 64-3.7-C0-NO. Table 3 includes detailed FEM results for each specimen.

The ultimate load increased significantly with increasing the prestressing reinforcement ratio. The prestressing reinforcement ratio played an obvious role in the level of capacity enhancement. Specimen 64-2-C0-NO, possessing the lowest reinforcement ratio of 0.002 in the test series, failed at an ultimate capacity of 84 kN, whereas specimens 64-2.7-C0-NO, 64-3.7-C0-NO, and 64-6.4-C0-NO failed at ultimate capacities of 110, 150, and 238 kN respectively. Thus, an increase of 180% was achieved when the prestressing reinforcement ratio increased from 0.002 to

0.0064.

Specimens 64-2.0-C0-NO and 64-2.7-C0-NO with reinforcement ratios of 0.002 and 0.0027, failed in flexure whereas specimens 64-3.7-C0-NO (Fig. 9) and 64-6.4-C0-NO with prestressing reinforcement ratios of 0.0037 and 0.0064, experienced a mixed mode of failure as flexural and shear cracks were distinctly visible during the failure stage of these specimens. These modes of failure are consistent with those reported by Foubert *et al.* (2016), Mahmoud *et al.* (2017).

5.3 Effect of strengthening using CFRP strips

In this test series, the effect of strengthening of the PHC slabs using 2, 3, 5 and 7 CFRP strips having a reinforcement area of 64, 96, 160, and 224 mm² is investigated for specimens with a concrete compressive strength of 64 MPa and different prestressing reinforcement ratios of 0.002, 0.0037 and 0.0064 (Table 4). Strengthening using NSM-CFRP strips provided higher ultimate capacity without excessive increase in mid-span deflection (Foubert *et al.* 2016). The load-deflection behavior is an indicator of the effect of varying external reinforcement ratio on the flexural stiffness of each test specimen (Fig. 9). It can be seen that strengthening the specimen had no effect on the pre-cracking stiffness while it enhanced the post-cracking stiffness. The enhancement of the post-cracking stiffness was significant in specimens with the lowest prestressing reinforcement ratio (0.002), but then decreased as the prestressing reinforcement ratio was further increased to 0.0037 and 0.0064. The increase in post-cracking stiffness is dependent on the provided area of the CFRP strips as evidenced by the post-cracking response of specimens 64-2-C2-NO, 64-2-C3-NO, and 64-2-C5-NO and 64-2-C7-NO. The cracking load was not affected by adding the NSM-CFRP strips to specimens with different prestressing reinforcement ratio. On the other hand, for all strengthened specimens with a prestressing reinforcement ratio of 0.002, the yielding load increased significantly (24%) by adding two strips while further increase in the CFRP strips did not enhance the yielding load. In specimens with 0.0037 and 0.0064, the yield load increased marginally compared to that of the control unstrengthened specimen when the CFRP strips were added (Table 4). The ultimate capacity was also significantly enhanced when the slab strengthened with 2, 3, 5 or 7 CFRP strips. Strengthening the specimens having prestressing reinforcement ratio of 0.002, 0.0037, and 0.0064 using 2 CFRP strips resulted in an increase in the ultimate load by 23, 18 and 9%, respectively. However, further increase in the CFRP strip to 3, 5 and 7, increased

Table 4 Specimen details and results for series III

Specimen	Prestressing reinforcement area, (mm ²)	NSM-CFRP Reinforcement area, (mm ²)	Cracking load, (kN)	Yielding load, (kN)	Ultimate Capacity, (kN)	Strain in the CFRP at ultimate, ($\mu\epsilon$)	Mode of Failure
64-2.0-C0-NO		0	64	78	84	-	F
64-2.0-C2-NO		64	68	82	98	4396	F
64-2.0-C3-NO	275	96	68	82	100	5156	F
64-2.0-C5-NO		160	68	82	104	3899	F
64-2.0-C7-NO		224	70	84	108	3610	F
64-3.7-C0-NO		0	108	132	150	-	F-S
64-3.7-C2-NO		64	112	136	177	7430	F-S
64-3.7-C3-NO	517	96	112	138	185	7445	F-S
64-3.7-C5-NO		160	114	140	190	6040	F-S
64-3.7-C7-NO		224	114	144	198	5656	F-S
64-6.4-C0-NO		0	146	178	238	-	F-S
64-6.4-C2-NO		64	148	180	260	5635	F-S
64-6.4-C3-NO	898	96	148	182	266	5939	F-S
64-6.4-C5-NO		160	148	184	276	6353	F-S
64-6.4-C7-NO		224	148	186	282	6117	F-S

Note: F = Flexural failure; F-S = Flexure-shear failure

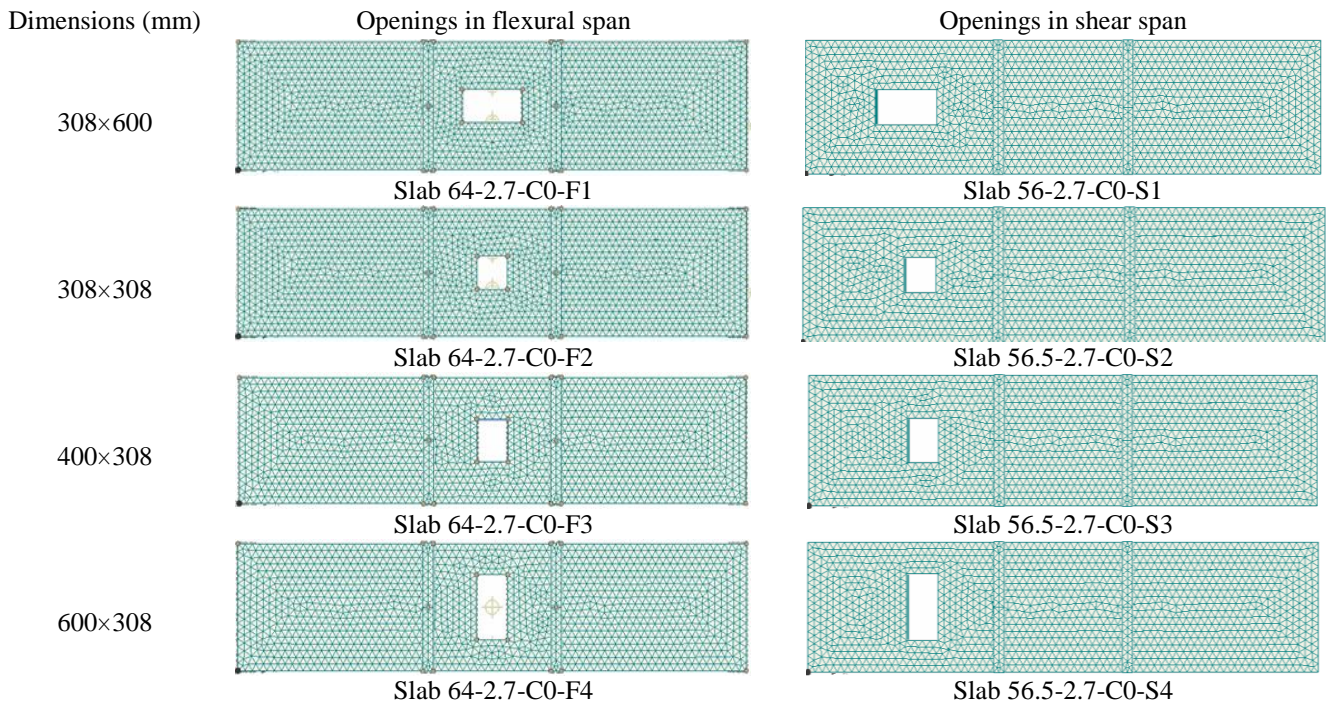


Fig. 10 Opening dimensions and locations

the ultimate load slightly (3% on average) in specimens with different prestressing reinforcement ratios when compared to slabs strengthened with 2 strips. In specimens with 0.002, 0.0037 and 0.0064 prestressing reinforcement ratios, an overall increase in ultimate capacity by 35, 32 and 18%, was observed when control unstrengthened slabs 64-2-C0-NO, 64-3.7-C0-NO and 64-6.4-C0-NO were provided with 7 CFRP strips, respectively. For specimens with the least prestressing reinforcement ratio of 0.002, the addition of CFRP strips for strengthening increased the flexural capacity; however, the mode of failure observed in all specimens with this prestressing reinforcement ratio was

flexural failure.

In specimens strengthened with CFRP strips, the experimentally-measured strains in the CFRP strips (Foubert *et al.* 2016) were used as a guide to determine whether the CFRP strips debonded/ruptured or not in the FEM specimens. In all strengthened slabs with prestressing reinforcement ratio of 0.002, the CFRP strains (Table 4) were much less than those reported by Foubert *et al.* (2016). This suggests that there was no rupture or debonding of the CFRP strips. Specimens with 0.0037 and 0.0064 prestressing reinforcement ratios exhibited flexure-shear failure mode. Despite the low strain in CFRP strips in these

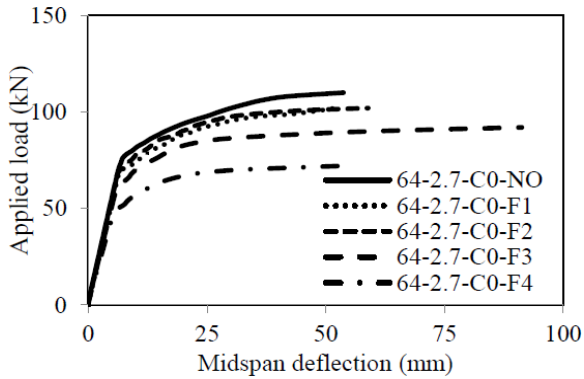


Fig. 11 Load-deflection relationship for effect of opening dimensions along flexural span

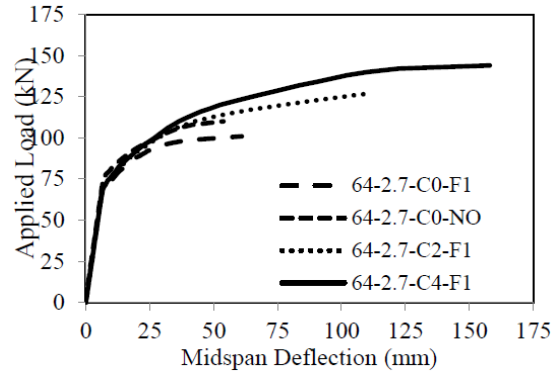


Fig. 12 Load-deflection relationship for strengthening of slabs with openings along flexural span

specimens, this mode of failure was accompanied with debonding of the CFRP strips due to the development of diagonal shear cracks (Foubert *et al.* 2016).

5.4 Effect of openings

The effect of openings with different sizes, located on either flexural or shear spans, on the behavior of PHC slabs was examined. Four different opening sizes were selected $308 \times 308 \text{ mm}^2$, $308 \times 600 \text{ mm}^2$, $400 \times 308 \text{ mm}^2$ and $600 \times 308 \text{ mm}^2$ as shown in Fig. 10. In all four cases, the effect of strengthening using either 2 or 4 NSM-CFRP strips was also evaluated. For slabs with opening in the shear span, the opening started at a distance equal to twice the member depth from the concentrated loading point to avoid any undesirable effects on the ultimate failure load.

5.4.1 Openings in the flexural span

An opening located within the flexural span had a detrimental effect on the flexural stiffness and cracking, yielding, and ultimate capacities. For slab 64-3.6-C0-F1, the opening that resulted in cutting only one strand ($308 \times 600 \text{ mm}^2$) caused a decrease in the cracking load, yielding and ultimate capacity by 10% compared to the control slab 64-

2.7-C0-NO without openings. To further investigate the effect of opening size, the dimension of the opening in the longitudinal direction of the slab was reduced from 600 to 308 mm. This change in length led to a square opening of size $308 \times 308 \text{ mm}^2$. This reduction in the length of opening did not show any significant change in the structural behavior of slab 64-2.7-C0-F2 in terms of cracking load, yielding and ultimate capacity compared to that of specimen 64-2.7-C0-F1 (Fig. 11). When the length of the opening, in the transverse direction of the slab, increased from 308 to 400 or 600 mm, three prestressing strands were cut. This resulted in significant reduction in both the pre-cracking and post-cracking stiffness. Also, the cracking load of slabs 64-2.7-C0-F3 and 64-2.7-C0-F4 decreased by 11.4 and 28.6% when compared to that of the control slab 64-2.7-C0-NO. Similarly, yielding, and ultimate capacity were reduced significantly in both slabs (Table 5) where slab 64-2.7-C0-F3 and 64-2.7-C0-F4 failed at an ultimate capacity of 92 and 72 kN, respectively, indicating a 20 and 35% decrease in ultimate capacity with respect to the control slab 64-3.6-C0-NO.

When slab 64-2.7-C0-F1 was strengthened with two CFRP strips, an increase in post-cracking stiffness was clearly observed (Fig. 12). The NSM-CFRP strips did not

Table 5 Specimen details and results for slabs with openings along flexural span

Specimen	Prestressing reinforcement area, (mm^2)	NSM-CFRP Reinforcement area, (mm^2)	Cracking load, (kN)	Yielding load, (kN)	Ultimate Capacity, (kN)	Strain in the CFRP at ultimate, ($\mu\epsilon$)	Mode of Failure
64-2.7-C0-F1		0	70	81	98	-	F
64-2.7-C2-F1		64	69	88	127	11,414	F
64-2.7-C4-F1		128	70	92	144	13,503	F
64-2.7-C0-F2		0	70	81	99	-	F
64-2.7-C2-F2		64	70	91	125	11,277	F
64-2.7-C4-F2		128	71	93	139	9,994	F
64-2.7-C0-F3	384	0	62	80	92	-	F
64-2.7-C2-F3		64	62	82	112	13,139	F
64-2.7-C4-F3		128	62	84	122	12,468	F
64-2.7-C0-F4		0	50	58	72	-	F
64-2.7-C2-F4		64	50	60	94	12,934	F
64-2.7-C4-F4		128	52	64	106	11,413	F

Note: F = Flexural failure; F-S = Flexure-shear failure

Table 6 Specimen details and results for slabs with openings along shear span

Specimen	Prestressing reinforcement area, (mm ²)	NSM-CFRP Reinforcement area, (mm ²)	Cracking load, (kN)	Yielding load, (kN)	Ultimate Capacity, (kN)	Strain in the CFRP at ultimate, ($\mu\epsilon$)	Mode of Failure
56-2.7-C0-S1	384	0	80	88	100	-	F-S
56-2.7-C2-S1		64	80	92	118	3861	F-S
56-2.7-C4-S1		128	80	94	136	8980	F-S
56-2.7-C0-S2		0	80	88	100	-	F-S
56-2.7-C2-S2		64	80	92	118	5551	F-S
56-2.7-C4-S2		128	80	94	138	10,935	F-S
56-2.7-C0-S3		0	72	NA	74	-	S
56-2.7-C2-S3		64	72	NA	80	940	S
56-2.7-C4-S3		128	74	92	98	1707	F-S
56-2.7-C0-S4		0	72	NA	74	-	S
56-2.7-C2-S4		64	72	86	88	1341	S
56-2.7-C4-S4		128	72	94	98	1708	F-S

Note: F = Flexural failure; F-S = Flexure-shear failure

have any effect on cracking load, which remained unchanged after the addition of two CFRP strips. An increase in ultimate capacity from 100 to 127 kN was achieved for slab 64-3.6-C2-F1; this increase in ultimate capacity was also observed experimentally (Mahmoud *et al.* 2017). Further, when two additional CFRP strips (total of 4) were used in slab 64-2.7-C4-F1, the increase in yielding and ultimate capacities was not directly proportional. An increase of 44% in the ultimate capacity was achieved for slab 64-3.6-C4-F1 with respect to slab 64-2.7-C0-F1. Similar trend was observed in slab 64-2.7-C0-F2 where the reduction of the length of the opening had no effect on the overall behavior. Moreover, strengthening slab 64-2.7-C0-F3 with two CFRP strips restored the entire capacity of slab that was lost due to introducing the opening. Furthermore, when four CFRP strips were used to strengthen slab 64-2.7-C0-F3, an improvement in ultimate capacity by 11 % was achieved, with regard to slab 64-2.7-C0-NO. In addition, strengthening slab 64-2.7-C0-F4 with two and four CFRP strips had a positive effect on increasing the post-cracking stiffness and ultimate capacity of the slab. The ultimate capacity of the slab witnessed an increase of 30 and 47% with the installation of two and four CFRP strips, respectively, when compared with the unstrengthened slab 64-2.7-C0-F4. Approximately the entire lost capacity due to the presence of an opening was restored when 4 CFRP strips were used. All specimens in this series failed in flexure where a distinctive yielding of steel reinforcement was observed. The addition of CFRP strips did not change this mode of failure. Again, based on the CFRP strains (Table 5), it can be said that debonding of the CFRP strips occurred as the strains were higher than those reported by Mahmoud *et al.* (2017). The debonding of the CFRP strips may be due to the cracks that propagated diagonally from the opening corner to the side of the slab.

5.4.2 Openings in the shear span

An opening located within the shear span did not have a significant impact on the slab pre-cracking stiffness as indicated by the similar stiffness of the slabs with and

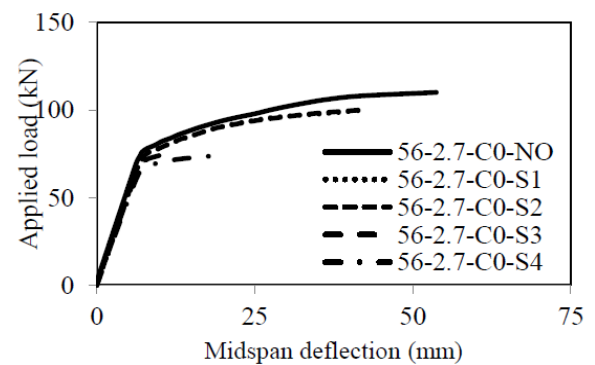


Fig. 13 Load-deflection relationship for effect of opening dimensions along shear span

without openings, while a slight decrease was observed in the post-cracking stiffness (Fig. 13). Also, insignificant decrease in the ultimate capacity of the test specimens (7%) was observed in specimens with an opening of 308×600 mm² and 308×308 mm² (Specimens 56-2.7-C0-F1 and 56-2.7-C0-F2) where their ultimate capacity was 100 kN. Specimen 56-3.6-S0-F4 having an opening size of 600×308 showed a decrease in the ultimate capacity by 32%, the highest decline among all the opening sizes tested in this series (Table 6). It should be noted here that all slabs with opening in the shear span failed due to shear before reaching their flexural capacity.

For all specimens strengthened with CFRP strips in this series, the cracking load was unaffected by the addition of CFRP strips. In general, the specimens strengthened with 2 strips achieved higher gain in the ultimate capacity with respect to their control slabs than specimens strengthened with 4 strips (Fig. 14). The increase in strength with the addition of CFRP strips is not directly proportional and a diminishing effect in this regard holds true. The addition of 2 CFRP strips for slab 56-2.7-C0-S1 and 56-2.7-C0-S2 restored the entire lost capacity due to the introduction of an opening and further enhancement in the ultimate capacity was achieved for these two slabs with addition of 4 CFRP strips. In case of slabs 56-2.7-C0-S3 and 56-2.7-C0-F4, the

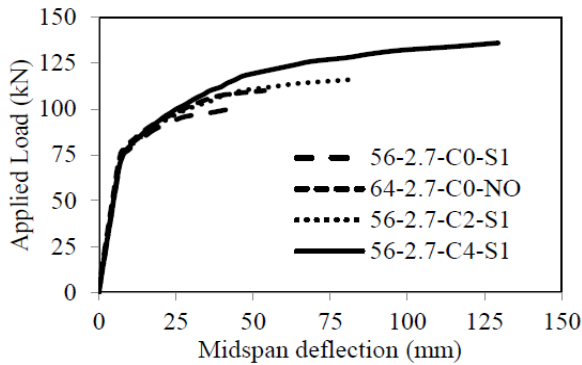


Fig. 14 Load-deflection relationship for strengthening of slabs along shear span

addition of 2 CFRP strips led to a shear failure at an ultimate capacity of 80 and 88 kN, respectively. Further, using 4 CFRP strips led to an increase in ultimate capacity but the slabs could not regain the entire lost capacity due to the presence of the openings. Yielding of prestressing reinforcement was delayed slightly for all specimens with strengthening. Specimens strengthened with 2 and 4 CFRP strips experienced a noticeable enhancement in post-cracking stiffness, and correspondingly significant enhancement in the corresponding yield loads, except for slabs having opening sizes of $400 \times 308 \text{ mm}^2$ and $600 \times 308 \text{ mm}^2$, as these slabs failed in shear. Specimens with opening size of $308 \times 600 \text{ mm}^2$ and $308 \times 308 \text{ mm}^2$ located within the shear span experienced flexure-shear failure where yielding of the strands was observed. Although the addition of CFRP strips increased the ultimate capacity, the mode of failure was flexure-shear failure associated with debonding of the CFRP strips (based on the same reasons mentioned earlier). Slabs 56-2.7-C0-S3 and 56-2.7-C0-S4 having opening size of $400 \times 308 \text{ mm}^2$ and $600 \times 308 \text{ mm}^2$ were critical in shear and failed in a brittle manner without experiencing any yielding of prestressing steel reinforcement. The addition of 2 CFRP strips to these two specimens increased their capacity but the mode of failure remained unchanged. However, addition of 4 CFRP strips changed the mode of

failure from a pure shear failure to a mixed shear-flexure mode of failure where yielding of steel reinforcement took place before final shear failure.

6. Comparison between numerical and code predicted capacities

Tables 7 and 8 present the numerical and code predicted flexural and shear capacities for all specimens. The flexural capacity of the unstrengthened slabs was calculated according to the Canadian standard CSA/A23.3-14 (CSA 2014) while that of strengthened slabs were calculated using the CSA/S806-12 (CSA 2012) without applying any modification factors, such as environmental and materials factors. This code has no specific shear design provisions for members strengthened in flexure; thus, the shear capacity was calculated according to the CSA/A23.3-14 (CSA 2014), neglecting the CFRP strips. The CSA/S806-12 (CSA 2012) specifies a maximum permissible strain in the NSM reinforcement of 0.007.

In the unstrengthened slabs with 0.002 prestressing reinforcement ratio (failed in flexure), the CSA/A23.3-14 gave reasonable predictions where the average FEM-to-predicted flexural capacity ratio was 0.98. Because slabs with higher reinforcement ratios failed in shear, the comparison was made in terms of shear strength. The CSA/A23.3-14 overestimated the shear capacity for slabs with 0.0037 prestressing reinforcement ratio where the average FEM-to-predicted shear capacity ratios was 0.9. For slabs with the highest reinforcement ratio (0.0064), shear forces at failure were significantly underestimated where the FEM-to-predicted shear capacity ratio was 1.45. It is worth mentioning that the flexural capacities at failure for slabs with 0.0037 and 0.0064 were very close to the predicted ones (1.03 on average).

In strengthened slabs with 0.002 prestressing reinforcement ratio, the CSA/S806-12 yielded an average FEM-to-predicted flexural capacity ratio of 1.0 with a coefficient of variation of 8.5%. In specimens with openings in the flexural span, the CSA/S806-12 produced

Table 7 FEM and code predicted flexural and shear capacities for series I and II

Series	Specimen	FEM		CSA Standards	
		Moment (kN.m)	Shear (kN)	Moment (kN.m)	Shear (kN)
I	64-2.0-C0-NO	72	40	78.0	78.8
	80-2.0-C0-NO	79.2	44	79.7	88.1
	100-2.0-C0-NO	82.8	46	81.2	98.5
	64-3.7-C0-NO	135	75	134.7	78.8
	80-3.7-C0-NO	144	80	137.3	88.1
	100-3.7-C0-NO	149.4	83	139.8	98.5
	64-6.4-C0-NO	214.2	119	218.8	78.8
	80-6.4-C0-NO	232.2	129	223.7	88.1
II	100-6.4-C0-NO	244.8	136	227.6	98.5
	64-2.0-C0-NO	72	40	78.0	78.8
	64-2.7-C0-NO	99	55	104.0	78.8
	64-3.7-C0-NO	135	75	134.7	78.8
	64-6.4-C0-NO	214.2	119	218.8	78.8

Table 8 FEM and code predicted flexural and shear capacities for series III, IV and V

Series	Specimen	FEM		CSA Standards	
		Moment (kN.m)	Shear (kN)	Moment (kN.m)	Shear (kN)
III	64-2.0-C0-NO	72	40	78.0	78.8
	64-2.0-C2-NO	88.2	49	80.9	78.8
	64-2.0-C3-NO	90	50	86.6	78.8
	64-2.0-C5-NO	93.6	52	92.4	78.8
	64-2.0-C7-NO	97.2	54	109.4	78.8
	64-3.7-C0-NO	135	75	134.7	78.8
	64-3.7-C2-NO	159.3	88.5	138.3	78.8
	64-3.7-C3-NO	166.5	92.5	143.5	78.8
	64-3.7-C5-NO	171	95	154.5	78.8
	64-3.7-C7-NO	178.2	99	165.5	78.8
	64-6.4-C0-NO	214.2	119	213.4	78.8
	64-6.4-C2-NO	234	130	223.9	78.8
	64-6.4-C3-NO	239.4	133	229.1	78.8
	64-6.4-C5-NO	248.4	138	239.6	78.8
	64-6.4-C7-NO	253.8	141	249.9	78.8
IV	64-2.7-C0-F1	88.2	49	81.0	78.8
	64-2.7-C2-F1	114.3	63.5	93.1	78.8
	64-2.7-C4-F1	129.6	72	105.2	78.8
	64-2.7-C0-F2	89.1	49.5	81.0	78.8
	64-2.7-C2-F2	112.5	62.5	93.1	78.8
	64-2.7-C4-F2	125.1	69.5	105.2	78.8
	64-2.7-C0-F3	82.8	46	54.6	78.8
	64-2.7-C2-F3	100.8	56	66.2	78.8
	64-2.7-C4-F3	109.8	61	77.9	78.8
	64-2.7-C0-F4	64.8	36	54.0	78.8
	64-2.7-C2-F4	84.6	47	65.6	78.8
	64-2.7-C4-F4	95.4	53	77.1	78.8
V	56-2.7-C0-S1	90	50	104.0	67.4
	56-2.7-C2-S1	106.2	59	104.0	67.4
	56-2.7-C4-S1	122.4	68	104.0	67.4
	56-2.7-C0-S2	90	50	104.0	67.4
	56-2.7-C2-S2	106.2	59	104.0	67.4
	56-2.7-C4-S2	124.2	69	104.0	67.4
	56-2.7-C0-S3	90	37	104.0	50.2
	56-2.7-C2-S3	106.2	40	104.0	50.2
	56-2.7-C4-S3	124.2	49	104.0	50.2
	56-2.7-C0-S4	66.6	37	104.0	44.5
	56-2.7-C2-S4	72	44	104.0	44.5
	56-2.7-C4-S4	88.2	49	104.0	44.5

Notes The flexural capacity is calculated according to CSA/S806-12 (CSA 2012) while the shear capacity is calculated according to the CSA A23.3-14 (CSA 2014-a).

For slabs with shear openings, the flexural capacity is calculated at mid-span section while the shear capacity is calculated at the opening

conservative predictions for the flexural capacity where the average FEM-to-predicted flexural capacity ratio was 1.29 with a coefficient of variation of 9.4%. For strengthened specimens with 0.0037 reinforcement ratio that failed in flexural-shear, the predictions were slightly conservative with an average FEM-to-predicted shear capacity ratio of 1.19 and a coefficient of variation of 4.7%. The predictions were more conservative in case of slabs with reinforcement ratio of 0.0064 where the average FEM-to-predicted shear capacity ratio was 1.72 with a coefficient of variation of

3.6%. In slabs with shear openings, the average FEM-to-predicted shear capacity ratio was 0.96 with a coefficient of variation of 9.0%.

7. Conclusions

A finite element model was constructed and validated against experimental test results previously conducted by the authors. The model was able to capture the general

behavior of PHC slabs with and without openings (unstrengthened and strengthened with NSM-CFRP strips). The validated FEM was used to run a parametric study to investigate the influence of several key factors affecting the behavior of such slabs including the prestressing reinforcement ratio, concrete compressive strength, NSM-CFRP reinforcement ratio and size and location of openings. Based on the numerical results and discussion, the following conclusions can be made:

- Increasing the compressive strength of concrete from 64 to 80 or 100 MPa resulted in a slight increase of 7 to 16% in the cracking load, 5 to 8% in the yielding load and 7 to 12% in the ultimate capacity.
- Increasing the prestressing reinforcement ratio from 0.002 to 0.0027 resulted in a substantial increase of 21% in the cracking load, 33% in the yielding load and 31% in the ultimate capacity. However, these percentages were 38 to 87%, 37 to 124%, and 36 to 116%, respectively, when the prestressing reinforcement ratio was increased from 0.0027 to 0.0037 and 0.0064.
- The installation of NSM-CFRP strips led to a significant improvement in the structural performance of the PHC slabs. Although the addition of NSM reinforcement had no effect on the cracking load, it increased the ultimate capacity significantly. An increase of 35% in the ultimate capacity was observed in specimens with low reinforcement ratio (0.002) compared to 18% in specimens with high reinforcement ratio (0.0064). The increase in the ultimate capacity of the slab was not directly proportional to the provided external reinforcement area. The ultimate capacity increased by 18, 23, 27 and 32% when slab 64-3.7-C0-NO (with prestressing reinforcement ratio of 0.0037) was strengthened with 2, 3, 5 and 7 strips.
- An opening located in the flexural span was detrimental to the capacity of the PHC slabs. The change in the opening dimension (from 308×600 to 308×308 mm²) in the longitudinal direction of the slab had insignificant effect on the ultimate capacity, while the change in the opening dimension in the transverse direction (from 308×600 to 600×308 mm²) resulted in a significant reduction in the ultimate capacity of the slab (approximately 35%).
- For strengthened specimens with openings in the flexure span, cracking simultaneously originated at the corners of the openings and at the mid-span, indicating that the NSM reinforcement effectively resisted the stresses developed at the opening and redistributed them along the reinforcement profile. Providing 2 or 4 NSM-CFRP strips (32 mm² each) was successful in restoring the original ultimate capacity of the slabs before introducing the opening. An enhancement of 31 and 26% in the ultimate capacities was observed for slabs with opening dimensions of 308×600 and 308×308 mm², respectively.
- Slabs with small openings in the shear span (308 mm width, cutting one strand) showed slightly lower capacity (9%), while those with larger openings (400 or 600 mm width, cutting two strands) experienced significant reduction (33%) in the ultimate capacity.

Strengthening openings (308×600 and 308×308 mm²) with 2 or 4 NSM-CFRP strips was able to restore the original capacity of the slab without openings. However, in slabs with 400×308 and 600×308 mm² openings, the 2 or 4 strips could only restore about 90 % of the original capacity of the slab.

- The CSA standards CSA/A23.3-14 (CSA 2014a) produced good predictions of the flexural capacity for unstrengthened PHC slabs failed in flexure with an average FEM-to-predicted flexural capacity ratio of 0.98. Also, for strengthened slabs, with or without openings that failed in flexure, the CSA/S806-12 (CSA 2012) yielded reasonable predictions of the flexural capacities with an average FEM-to-predicted flexural capacity ratio of 1.15. Moreover, for unstrengthened slabs with low reinforcement ratio, failed in shear, the CSA/A23.3-14 predicted reasonably their shear capacities, with an average FEM-to-predicted shear capacity ratio of 0.9, while it was conservative in slabs with high reinforcement ratio (0.0064) with an average FEM-to-predicted shear capacity ratio of 1.45. Similar trend was observed in NSM-CFRP strengthened PHC slabs.

Acknowledgements

The financial support provided by the Natural Science and Engineering Research Council of Canada (NSERC) is gratefully appreciated.

Reference

- Al-Saadi, N.T.K and Al-Mahaidi, R. (2016), "Modelling of NSM CFRP strips embedded in concrete using lap shear tests with epoxy adhesive", *J. Compos. Struct.*, **153**, 662-672.
- Al-Saadi, N.T.K. and Al-Mahaidi, R. (2016), "Modelling of near-surface mounted carbon fibre reinforced polymer strips embedded in concrete with cement-based adhesive", *Constr. Build. Mater.*, **127**, 383-393.
- Barros, J.A.O., Dias, S.J.E. and Lima, J.L.T. (2007), "Efficacy of CFRP-based techniques for the flexural and shear strengthening of concrete beams", *Cement Concrete Compos.*, **29**(3), 203-217.
- Bigaj, A. (1999), "Structural dependence of rotation capacity of plastic hinges", PhD Thesis, Department of civil engineering, Delft University of Technology, Delft, Netherlands.
- Cervenka, V., Jendele, L. and Cervenka, J. (2016), *ATENA Program Documentation Part 1: Theory*, Cervenka Consulting Ltd., Prague, Czech Republic.
- CSA (2012), Design and Construction of Building Structures with Fibre-Reinforced Polymers, CSA/S806-12, Canadian Standards Association, Toronto, Ontario, Canada.
- CSA (2014a), Code for the Design of Concrete Structures for Buildings, CSA/ A23.3-14, Canadian Standards Association, Toronto, Ontario, Canada.
- CSA (2014b), Canadian Highway Bridge Design Code, CSA/S6-14, Canadian Standards Association, Toronto, Ontario, Canada.
- De Lorenzis, L., Nanni, A. and La Tegola, A. (2000), "Strengthening of reinforced concrete structures with near surface mounted FRP rods", *International Meeting on Composite Materials, PLAST 2000, Proceedings, Advancing with Composites*, Milan, Italy, May.

- Elgabbas, F., El-Ghandour, A.A., Abdelrahman, A.A. and El-Dieb, A.S. (2010), "Different CFRP strengthening techniques for prestressed hollow core concrete slabs: experimental study and analytical investigation", *Compos. Struct.*, **92**(2), 401-411.
- Enochsson, O., Lundqvist, J., Taljsten, B., Rusinowski, P. and Olofsson, T. (2007), "CFRP strengthened openings in two-way concrete slabs-An experimental and numerical study", *Constr. Build. Mater.*, **21**(4), 810-826.
- fib Bulletin 14 (2001), "Externally bonded FRP reinforcement for RC structures, Fédération Internationale du Béton", Switzerland.
- Foubert, S. (2015), "Flexural strengthening of prestressed hollow core slabs using NSM-FRP technique", MSc Thesis, University of Manitoba, Winnipeg, MB, Canada.
- Foubert, S., Mahmoud, K. and El-Salakawy, E. (2016), "Behavior of prestressed hollow-core slabs strengthened in flexure with near-surface mounted carbon fiber-reinforced polymer reinforcement", *J. Compos. Constr.*, **20**(6),.
- Hassan, T.K. and Rizkalla, S.H. (2003), "Investigation of bond in concrete structures strengthened with near surface mounted carbon fiber reinforced polymer strips", *J. Compos. Constr.*, **7**(3), 248-257.
- ISIS Canada (2007), "Reinforcing concrete structures with fibre reinforced polymers", *Intelligent Sensing for Innovative Structures*, Winnipeg, Manitoba, Canada.
- Khajehdehi, R. and Panahshahi, N. (2016), "Effect of openings on in-plane structural behavior of reinforced concrete floor slabs", *J. Build. Eng.*, **7**, 1-11.
- Kim, S., Riyad, S. and Aboutaha, R.S. (2004), "Finite element analysis of carbon fiber-reinforced polymer (CFRP) strengthened reinforced concrete beams", *Comput. Concrete*, **1**(4), 401-416.
- Mahmoud, K., Foubert, S. and El-Salakawy, E. (2017), "Strengthening of prestressed concrete hollow-core slab openings using near-surface-mounted carbon fiber-reinforced polymer reinforcement", *PCI J.*, **62**(4), 61-73.
- Mousavi, S.S. and Dehestani, M. (2015), "Implementation of bond-slip effects on behaviour of slabs in structures", *Comput. Concrete*, **16**(2), 311-327.
- Täljsten, B., Carolin, A. and Nordin, H. (2003), "Concrete structures strengthened with near surface mounted reinforcement of CFRP", *Adv. Struct. Eng.*, **6**(3), 201-213.
- Teng, J.G., De Lorenzis, L., Wang, B., Li, R., Wong, T.N. and Lam, L. (2006), "Debonding failures of RC beams strengthened with near surface mounted CFRP strips", *J. Compos. Constr.*, **2**(92), 92-105.
- Zhang, S.S., Teng, J.G. and Yu, T. (2013), "Bond-slip model for CFRP strips near-surface mounted to concrete", *Eng. Struct.*, **56**, 945-953.

CC

Appendix

Design procedure for Specimen I-1-S2-NO

Flexural Capacity-Strain Compatibility Method [CSA/S806-12]

$$\alpha_1 = 0.85 - 0.0015f'_c \geq 0.67$$

$$\alpha_1 = 0.85 - 0.0015(56.5) = 0.765$$

$$\beta_1 = 0.97 - 0.0025f'_c \geq 0.67$$

$$\beta_1 = 0.97 - 0.0025(56.5) = 0.829$$

$$C = T_p + T_{FRP}$$

$$\alpha_1 f'_c \beta_1 c b_f = A_p f_{pr} + \varepsilon_{FRP} E_{FRP} A_{FRP}$$

The CSA/806-12 (CSA 2012) recommends that a maximum allowable strain in the NSM-FRP be 0.007 (Clause 11.3.1.3).

$$\begin{aligned} & (0.765)(56.5)(0.829)(1200)c \\ & = 383.6f_{pr} + (0.007)(131000)(2 \times 32) \\ & \quad c = 0.0089f_{pr} + 1.37 \\ & \quad \varepsilon_{pr} = \varepsilon_{pe} + \varepsilon_{ce} + \varepsilon_{su} \\ & \varepsilon_{pe} = \frac{f_{sj} - \Delta_{FS1}}{E_p} = \frac{1395 - 183.3}{195000} = 0.0062 \\ & \quad \varepsilon_{ce} = \text{negligible} \\ & \quad \frac{\varepsilon_{su}}{158 - c} = \frac{0.007}{203 - c} \\ & \varepsilon_{su} = \frac{(158 - c)(0.007)}{203 - c} = \frac{1.106 - 0.007c}{203 - c} \\ & \varepsilon_{pr} = 0.0062 + \frac{1.106 - 0.007c}{203 - c} \end{aligned} \quad (1)$$

$$\begin{aligned} f_{pr} &= (190 \times 10^3) \varepsilon_{pr} \left\{ 0.025 + \frac{0.975}{\left[1 + (118\varepsilon_{pr})^{10} \right]^{0.1}} \right\} \\ &\leq 1860 \text{ MPa} \end{aligned} \quad (2)$$

$$c = 0.0089f_{pr} + 1.37 \quad (3)$$

Iterations using Eqs. (1), (2) and (3)

$$\text{Try: } \varepsilon_{pr} = 0.012 \rightarrow f_{pr} = 1622.15 \text{ MPa} \rightarrow$$

$$c = 15.81 \text{ mm} \rightarrow \varepsilon_{pr} = 0.0115$$

$$\text{Try: } \varepsilon_{pr} = 0.0115 \rightarrow f_{pr} = 1617.31 \text{ MPa} \rightarrow$$

$$c = 15.76 \text{ mm} \rightarrow \varepsilon_{pr} = 0.0115 \text{ Ok.}$$

Check:

$$\frac{\varepsilon_c}{c} = \frac{\varepsilon_{FRPu}}{h - c} \text{ where } \varepsilon_c < \varepsilon_{cu} = 0.0035$$

$$\frac{\varepsilon_c}{15.76} = \frac{0.007}{203 - 15.76} \text{ where } \varepsilon_c = 0.0006 < 0.0035 \text{ Ok.}$$

$$a = \beta_1 c = 0.829(15.76) = 13.1 \text{ mm}$$

$$M_r = A_p f_{pr} \left(d - \frac{a}{2} \right) + \varepsilon_{FRP} E_{FRP} A_{FRP} \left(h - \frac{a}{2} \right)$$

$$M_r = 94.0 + 11.5 = 105.5 \text{ kN.m}$$

Shear capacity - Simplified method [CSA S806-12]

$$V_c = \phi_c \lambda \beta \sqrt{f'_c} b_w d_v \quad \text{where } \sqrt{f'_c} \leq 8.0 \text{ MPa}$$

Where $\phi_c = 1.0$, $\lambda = 1.0$

$\beta = 0.21$ (clause 11.3.6.2.a)

$d_v =$ the greater of $0.9d = 142.2$ mm or $0.72d = 146.16$ mm, thus $d_v = 146.16$ mm

$b_w =$ width of webs = 330 mm

$V_c = 0.65 \times 1.0 \times 0.21 \times 7.48 \times 146.16 \times 330 / 1000 = 76$ kN.